Journal of Computational Physics 228 (2009) 4757–4772

Contents lists available at ScienceDirect

Journal of Computational Physics

journal homepage: www.elsevier.com/locate/jcp

Acoustic modeling of perforated plates with bias flow for Large-Eddy Simulations ☆

S. Mendez [a,*], J.D. Eldredge [b]

[a] CERFACS, 42 av. G. Coriolis, 31057 Toulouse, France
[b] Mechanical and Aerospace Engineering Department, University of California, Los Angeles, Los Angeles, CA 90095, USA

ARTICLE INFO

Article history:
Received 11 January 2009
Received in revised form 20 March 2009
Accepted 20 March 2009
Available online 29 March 2009

Keywords:
Perforated walls
Acoustic absorption
Large-Eddy Simulations
Time-domain acoustic modeling

ABSTRACT

The study of the acoustic effect of perforated plates by Large-Eddy Simulations is reported. The ability of compressible Large-Eddy Simulations to provide data on the flow around a perforated plate and the associated acoustic damping is demonstrated. In particular, assumptions of existing models of the acoustic effect of perforated plate are assessed thanks to the Large-Eddy Simulations results. The question of modeling the effect of perforated plates is then addressed in the context of thermo-acoustic instabilities of gas turbine combustion chambers. Details are provided about the implementation, validation and application of a homogeneous boundary condition modeling the acoustic effect of perforated plates for compressible Large-Eddy Simulations of the flow in combustions chambers cooled by full-coverage film cooling.

1. Introduction and objectives

Nowadays, competitive gas turbines have to prove a low pollutant emission capability. For example, Lean Premixed Prevaporized (LPP) systems are being developed [24,43] to take advantage of the lean combustion regime in terms of pollutants production, especially nitrogen dioxide [22]. However, LPP burners are likely to be subject to combustion instabilities [23,34], which consist in an unfavorable coupling between acoustics and combustion. Hence, the prediction of combustion instabilities necessitates an accurate description of both the unsteady combustion process and the acoustic modes in the chamber. Notably, in aeronautical gas turbines, one needs to consider the fact that liners are perforated. Indeed, to ensure their thermal protection, combustion chamber liners are often perforated with thousands of small holes (of diameter approximately 0.5 mm), through which air flowing in the casing is injected [22,28]. In the combustion chamber, the jets issuing from the holes coalesce in the vicinity of the wall, resulting in a cooling film that isolates the plate from the hot gases. This cooling system is known as full-coverage film cooling (FCFC) and is known to be very efficient.

From an acoustic point of view, the behavior of perforated plates is known to be very different from the one of a solid wall, even at small open-to-total area ratio. First, perforated plates are communications between the combustion chamber and the casing, which is likely to influence the acoustic modes of the complete chamber. Moreover, it has been demonstrated, both analytically [14,15], experimentally [12,17,48] and numerically [10,11] that perforated plates have a damping effect on incident acoustic waves and thus potentially on combustion instabilities. The sound attenuation mechanism consists in the con-

☆ Sections 1 and 2 are partly based on AIAA-paper 2008-3007, from J. Dassé, S. Mendez and F. Nicoud. (Ref. [10] in the present article). The common material is reprinted with permission of the American Institute of Aeronautics and Astronautics, Inc.

* Corresponding author. Present address: Center for Turbulence Research, Stanford University, 488 Escondido Mall, Stanford, CA 94305-3035, USA. Tel.: +1 650 723 0546.
E-mail address: smendez@stanford.edu (S. Mendez).

0021-9991/$ - see front matter © 2009 Elsevier Inc. All rights reserved.
doi:10.1016/j.jcp.2009.03.026

version of acoustic energy into vortical energy [1,14,46]: incident waves interact with the shear layers formed at the apertures rims; subjected to pressure fluctuations, the shear layers destabilize to form vortex rings. The vortices are then dissipated with insignificant broadband sound production. For certain frequencies, depending on the geometrical and operating characteristics, an incident acoustic wave can be almost completely damped by a system composed by a perforated liner and a back wall [2,17], which is exactly what is encountered in combustion chambers, the back wall being the wall bounding the casing. Moreover, perforated liners are also effective to absorb sound of grazing acoustic waves [12]. Grazing acoustic waves are characteristic of both longitudinal and azimuthal modes, which are the most energetic modes in combustion chambers.

Recently, the ability of Large-Eddy Simulations (LES) and Helmholtz solvers to study combustion instabilities has been proven [4,26,30,32,38,40,41,43]. In any of these approaches, the acoustic impact of multi-perforated liners is generally neglected: the direct representation of FCFC is out of reach in numerical simulations, due to the small size of the perforations relative to the resolved length scales in the flow. The problem is exactly the same from the dynamical point of view: to account for effusion cooling, Boudier et al. [3,4] have used a uniform model [27] recently developed from wall-resolved LES [28], avoiding the resolution of the effusion holes. Similarly, to improve the acoustics prediction, the influence of the perforated plate should be modeled in the numerical simulations. This objective can be reached in two steps:

- Perforated plates models have to be adapted to the configuration encountered in combustion chambers. Typical configurations involve a mean flow through the plate (bias flow) and a crossflow tangential to the plate on each side of it (grazing flow). Some existing models include the presence of bias flow through the plate [2,14,16,17,20,25,44]. Among them, some also account for the grazing flow [16,20,44]. However, these models are not *a priori* adapted to the geometry of the effusion cooling holes. In combustion chambers, perforations are generally inclined and the length-to-diameter ratio is more than unity: typically, perforations are inclined at 30° to the wall, with a diameter of 0.5 mm and a plate thickness of 1 mm, approximately. To the authors' knowledge, this kind of configuration have only received recent interest [11]. In FCFC, high temperature gradients are also observed in the apertures and the frontiers of the jets. This may also have an influence on the acoustic–vortex interaction.
- Once an appropriate model is available, it is necessary to implement it in the target numerical code. This can be challenging and depends on the nature of the code. Notably, impedances of perforated plates are complex and depend on the frequency of the acoustic excitation, which is difficult to reproduce in temporal codes [45,13]. As far as Helmholtz solvers are concerned, this increases the non-linearity of the eigenvalue problem to be solved.

This paper focuses on both aspects. In order to build models adapted to combustion chamber situations, it proves useful to rely on relevant data. One long-term objective of this study is to use wall-resolved Large-Eddy Simulations to generate numerical data for the development of acoustic models. The first objective of this paper is thus to establish the ability of wall-resolved LES to produce numerical data for perforated plate-acoustic interaction problems. This is achieved by calculating a classical configuration of acoustic–vortex interaction in perforated plates, corresponding to the analytical and experimental study by Bellucci et al. [2]. On the other hand, Mendez and Nicoud [27] have proposed a uniform model to account for the dynamical effect of effusion cooling on the main flow from previous wall-resolved LES [28]. As already stated, this model has been used in LES of the flow in realistic full-scale combustion chambers [3,4]. In the context of combustion instabilities the model that couples both sides of the perforated plates has to show an acceptable behavior in terms of response to acoustic perturbations. The second objective of this paper is to assess the quality of the acoustic response of the existing model and to propose a practical modification to improve it.

Section 2 is dedicated to the description of the LES of the acoustic response of a perforated plate in presence of bias flow. The LES code is first presented. Note that this code is also the target code for the implementation of models for multi-perforated walls. The configuration of interest is detailed and existing models to estimate this response are also presented, together with the reference experiment of Bellucci et al. [2] The LES results are then analyzed. Section 3 is dedicated to the modeling of multi-perforated plates in the time-domain. An analytical analysis, together with *a posteriori* testing, will be presented. A practical formulation will be provided to model multi-perforated plates in compressible Large-Eddy Simulations, with a satisfactory acoustic behavior. Section 4 ends the paper by providing results about the impact of accounting for perforated plates in compressible LES of the flow in an actual combustion chamber cooled by the full-coverage film cooling technique.

2. LES of the acoustic response of a perforated plate with bias flow

2.1. Presentation of the computation

2.1.1. The LES code

All simulations presented in the paper are carried out with the LES code developed at CERFACS, named AVBP (www.cerfacs.fr/cfd/avbp_code.php). It is a cell-vertex/finite element code, explicit in time, which solves the compressible Navier–Stokes equations on unstructured meshes for the conservative variables (mass density, momentum and total energy). AVBP is dedicated to Large-Eddy Simulations and Direct Numerical Simulations and has been widely used and validated in the past years in all kinds of configurations [28,29,35,37–39]. The numerical scheme is the TTGC (Two-step Taylor Galerkin C) scheme [6]: this essentially non-dissipative scheme was specifically developed to handle unsteady turbulent flows with unstruc-

tured meshes. It is third order accurate in both space and time. Note that the short computations presented further in Section 3 are performed using the finite volume Lax–Wendroff scheme [39] (second order accurate in space and time). For boundary conditions, the Navier–Stokes Characteristic Boundary Conditions (NSCBC) method of Poinsot and Lele [33] is used. For the simulations of the flow around a perforated plate (present section), the WALE subgrid model [31] is used. This model has the advantage of vanishing naturally in the zones of pure shear, so that it does not prevent a low-Reynolds number flow from transitioning to turbulence. In Section 4, the classical Smagorinsky model is used [42], with a constant fixed at $C_S = 0.18$.

2.1.2. Numerical configuration of interest

The configuration of interest is inspired by the experimental test rig studied by Bellucci et al. [2]. In their experiment, a cylindrical tube is closed at one of its ends by a wall. At a distance l from this wall, is placed a perforated plate, parallel to the back wall (normal to the tube axis). A bias flow through the perforated plate is generated by injecting air in the cavity formed by the perforated plate and the back wall, through orifices in the lateral wall of the tube, near the back wall. On the other side of the tube, four acoustic drivers generate an acoustic wave. Six microphones are used to measure the acoustic wave reflected by the plate. This configuration is representative of the situation encountered in combustion chambers. In a combustion chamber, the perforated plate is the chamber liner and the back wall is the wall bounding the casing. The cavity between the perforated plate and the back wall would be the casing. The perturbation generated by the loud speaker would correspond to an acoustic perturbation coming from the chamber, for example due to unsteady combustion.

Calculating exactly this configuration is out of reach because of the number of holes of the perforated plate. To compute this configuration, it has thus been decided to consider the situation where the perforated plate and the back wall are infinite. In this case, due to the periodicity of the perforations arrangement, the infinite configuration allows the use of periodic boundary conditions in the lateral frontiers of the computational domain. We then consider a unique perforation as shown in Fig. 1 that represents the computational domain used in the LES. Except from the periodicity in the calculation, the geometrical characteristics of the experiment are reproduced.

The geometrical characteristics of the plate are the following: the thickness of the plate is $h = 1.5$ mm, the holes diameter is $2a = 6$ mm and the perforations are separated by $d = 35$ mm in both directions. Perforations are arranged following an in-line arrangement. The porosity of the plate is thus $\sigma = \pi a^2/d^2 = 0.0231$. The holes direction is normal to the plate. In the experiment, the back wall is located at $l = 95$ mm from the perforated plate. The origin of the axes $(x = 0, y = 0, z = 0)$ is located at the center of the hole outlet. In the operating point we consider, a bias flow is present through the perforated plate. The bulk velocity in the holes is denoted by $\overline{U_j}$ (the overline operator denotes a time-average).

In the reference experiment, fluid is injected laterally, through the walls of the tube. In the calculations, this cannot be done. The back wall is replaced by an inlet boundary condition. To ensure a bias flow through the hole at bulk velocity $\overline{U_j}$, the air is injected at $u^\infty = \overline{U_j}\sigma$ through the inlet boundary condition. The inlet being fully reflecting, it behaves like a wall from an acoustic point of view. An outlet boundary condition closes the domain at $x = L = 3l$. L is chosen large enough to avoid spurious interactions between the outlet condition and the zone of interest. The computational grid is composed by 280,000 tetrahedra, 20 points describing the diameter of the hole.

The operating point is such that $\rho = 1.2$ kg m^{-3} and $\overline{U_j} = 5$ m s^{-1}, so that $u^\infty \approx 0.115$ m s^{-1}. The mean pressure at the outlet is 101,300 Pa and the gas injected is the air. The Mach number in the orifice is of order 0.015 and the Reynolds number in the aperture, based on the diameter and $\overline{U_j}$, is approximately 2000. For this operating point, the pressure loss in the perforation is 37 Pa, resulting in a discharge coefficient through the plate of $C_D = \sqrt{\rho \overline{U_j}^2/2\Delta P} = 0.64$. To assess the acoustic response of the system, the pressure at the outlet condition is pulsed by adding a sinusoidal perturbation to the reference state, with an amplitude of 5 Pa and at a frequency $f \in [250, 500$ Hz] (one simulation each 50 Hz). The Strouhal number of the configuration is defined from the frequency of excitation and the bulk velocity in the hole: $St = \frac{2\pi f a}{\overline{U_j}}$. Pulsed simulations last 30 excitation periods and the last 20 periods are used for post-processing purposes.

Note that the forcing method is slightly different from the one used in the neighboring works of Eldredge et al. [11]: in this LES investigation of the acoustic behavior of a perforated liner with tilted apertures, Eldredge et al. [11] use an incompressible code and force the inflow velocity condition by adding a small sinusoidal perturbation. The pressure fluctuations are measured at the inflow and outflow boundaries to compute the Rayleigh conductivity.

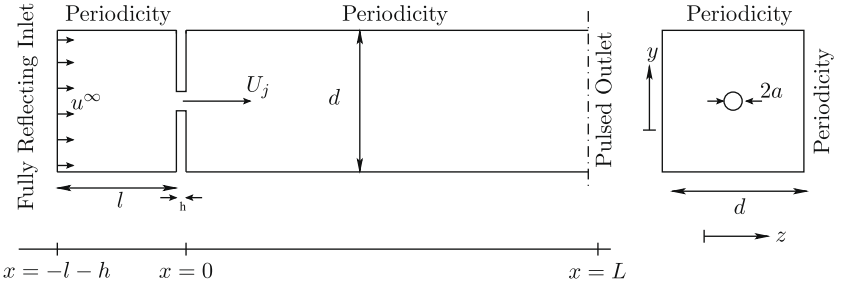

Fig. 1. Schematic of the configuration of interest. Computational domain for the LES. Figure from Dassé et al. [10].

2.2. Reference data: impedance models and reference experimental set up

In Section 2.3, the computational results will be presented. The numerical simulations will be compared to several data, either coming from experimental, numerical or analytical work. In particular, three models will be used. In the present section, the aim is to briefly summarize the hypotheses and the results of these models.

All models presented in this section are related to the work of Howe [14]. Howe proposed a model for linear sound absorption through a perforated plate. Indeed, in presence of bias flow and for acoustic perturbations of small amplitude, the mechanism is linear. Note that sound absorption occurs with and without mean flow through the aperture. In absence of mean flow through the aperture, the interaction is non-linear, the shear layer being created by the acoustic perturbation itself [9,46].

Assuming that acoustic–vortex interaction was the mechanism responsible for sound absorption, Howe built a model to evaluate the amount of energy transferred from acoustic to vortical energy. His results were notably confirmed by the subsequent experiments of Hughes and Dowling [17] and Eldredge and Dowling [12]. Three models are presented in the next paragraphs. First, the Howe model is discussed. Then a modified version [18] of this model is presented, accounting for the thickness of the plate, supposed to be zero in the Howe model. At last, the numerical model of Jing and Sun [19] is presented. This model solves the equations derived by Howe but in a more complex domain: Jing and Sun [19] include a finite plate thickness and a complex form for the jet separation at the aperture inlet. All these models give satisfactory results in the cited references.

2.2.1. Howe model (HM)

Howe's model for linear sound absorption by perforated screens in presence of bias flow has become classical, and is very often used for the construction of more elaborate models. The model developed by Howe [14] (HM) assumes an infinitely thin wall and a high Reynolds number in the aperture. It also considers that d/a (hole spacing-to-radius ratio) is large so that apertures do not interact with each other. A small perturbation is applied to the mean flow corresponding to the passage of fluid through the plate. Howe introduces harmonic variations at angular frequency $\omega = 2\pi f$ for the perturbation quantities (pressure p, velocity v and volume flux through the aperture q):

$$p = \Re[\hat{p}(x)exp(-i\omega t)], \quad u = \Re[\hat{u}(x)exp(-i\omega t)], \quad q = \Re[\hat{q}(x)exp(-i\omega t)], \tag{1}$$

where $\hat{p}$ is the amplitude of pressure fluctuations, $\hat{u}$ is the amplitude of velocity fluctuations and $\hat{q}$ the amplitude of the flow rate fluctuations through the aperture. $\Re$ denotes the real part of a complex number.

The acoustic behavior of an aperture is described through its Rayleigh conductivity K_R, which is defined as

$$K_R = \frac{i\rho\omega\hat{q}}{\hat{p}_+ - \hat{p}_-}, \tag{2}$$

where ρ is the mean density near the aperture and $\hat{p}_-$ and $\hat{p}_+$ the amplitudes of pressure fluctuations, measured below $(x < 0, \hat{p}_-)$ and above the aperture $(x > 0, \hat{p}_+)$.

At the rim of the aperture, the flow separates, forming a jet. The vorticity is supposed to be concentrated in an axisymmetric vortex sheet separating two regions of potential flow, the jet and the remainder of the domain. The acoustic perturbation pulses the vortex sheet, resulting in the periodical shedding of vortex rings. The vortex shedding is supposed to have the following characteristics: the vortex rings shed are assumed to have the diameter of the aperture and to be convected at the mean velocity in the aperture, $\overline{U_j}$. Under these hypotheses and assessing the strength of the vortex sheet using a Kutta condition, Howe determined the following expression of the Rayleigh conductivity:

$$\begin{aligned} &K_R = 2a(\gamma - i\delta) \\ &\text{with} \quad \gamma - i\delta = 1 + \frac{\frac{\pi}{2} I_1(St)e^{-St} - iK_1(St)\sinh(St)}{St\left[\frac{\pi}{2} I_1(St)e^{-St} + iK_1(St)\cosh(St)\right]}, \end{aligned} \tag{3}$$

where I_1 and K_1 are modified Bessel functions of the first and second kinds.

Note that a simpler version of the Howe model has been proposed by Luong et al. [25]. This will be discussed later in Section 3.

2.2.2. Howe model: modified version to account for the plate thickness (MHM)

As already stated, the model developed by Howe is relevant to infinitely thin plates. To account for the finite (but small) thickness of the plate, the Rayleigh conductivity derived by Howe is modified by adding a term representing the effect of plate thickness. This model can be found in several references, notably in papers by Jing and Sun [18,19] and gave good results in these studies and also with tilted apertures [11]. The Rayleigh conductivity in the modified version of the Howe model (MHM) is written:

$$K_R = 2a\left(\frac{1}{\gamma - i\delta} + \frac{2}{\pi}\frac{h}{a}\right)^{-1}. \tag{4}$$

2.2.3. Jing and Sun numerical model (JSM)

Jing and Sun [19] developed a numerical model (JSM) that solves the equations derived by Howe within a more complex geometry. In particular, the absence of plate thickness and the assumption of a cylindrical vortex sheet of diameter $2a$ allows Howe to find an analytical expression for K_R. The model proposed by Jing and Sun [19] includes a finite plate thickness and assumes a complex form for the vortex sheet. They used a previous study assessing the trajectory of the jet separation through axially symmetrical orifices [36]. By interpolation of the profiles given by this study, Jing and Sun [19] know the form of the vortex sheet, that is no more cylindrical. As a consequence, it is no more possible to derive an analytical solution. The governing equations are solved with the boundary element method. In this model, the convection velocity of the shed vortices is still supposed to be equal to the bulk velocity in the orifice, U. Results of the JSM for the case of interest ($h = 0.5a$) can be found in the recent study by Lee et al. [21].

2.2.4. Presentation of the reference data: reflection coefficient of the system

From the Rayleigh conductivity, one can build the impedance of the perforated plate $z_p = (\hat{p}_+ - \hat{p}_-)/\hat{u}(0)$, where $\hat{u}(0)$ stands for the amplitude of the velocity fluctuations in the direction normal to the plate, homogenized over the perforated wall ($\hat{q} = d^2\hat{u}$):

$$z_p = \frac{i\omega\rho d^2}{K_R}. \tag{5}$$

Assuming planar wave propagation between the perforated plate and the back wall, the cavity impedance reads:

$$z_c = -\frac{i\rho c}{\tan(kl)}, \tag{6}$$

with k the wave number of the perturbation and c the speed of sound. The total impedance of the system perforated plate-back cavity is thus

$$z_t = z_p + z_c = \frac{i\omega\rho d^2}{K_R} - \frac{i\rho c}{\tan(kl)} = i\rho\omega\left(\frac{d^2}{K_R} - \frac{1}{k\tan(kl)}\right). \tag{7}$$

The reflection coefficient of the whole system perforated plate-back wall is derived from this expression using

$$R = \frac{z_t + \rho c}{z_t - \rho c}. \tag{8}$$

The reflection coefficient is the quantity measured in the calculations, comparing the wave reflected by the system and the perturbation wave, imposed at the outlet boundary condition. These results are also compared to the experimental reflection coefficient of Bellucci et al. [2], using the absorption coefficient [17] $A = 1 - |R|^2$ and the phase of the reflection coefficient $\Phi(R)$.

2.3. Results and discussion

2.3.1. Flow visualization

Fig. 2 presents velocity and vorticity fields, the outlet pressure being pulsed at $f = 250$ and 400 Hz, respectively, over the cutting plane $z = 0$. Due to the section restriction, a jet is formed in the hole. At the hole inlet, the flow separates, forming a small recirculation close to the aperture edges (Fig. 2(a)). A shear layer is formed between the jet and the remainder of the flow. In both calculations, the jet issuing from the hole is pulsed and vortices are formed at the edges of the jet: the shear layer rolls up and forms vortices that are convected by the jet. This mechanism, responsible of the acoustic absorbing behavior of the perforated plate is reproduced in our simulations.

The global behavior at the two frequencies are identical but Fig. 2 shows that the jet does not react in the same manner, depending on the frequency of the forcing. At $f = 250$ Hz, the jet remains more coherent and is less sensitive to the pressure fluctuations. In Fig. 2(b), the shear layer rolls up $6a$ apart from the plate at $f = 250$ Hz and only $4a$ apart from the plate at $f = 400$ Hz. The same behavior is observed in Fig. 2(a). The jet destabilizes more easily at $f = 400$ Hz. The fields presented in Fig. 2 are instantaneous snapshots but they are representative of the general flow behavior. The differences in the hydrodynamic behaviors also induce differences in the acoustic response.

2.3.2. Acoustic results

Far enough from the plate, the acoustic waves reflected by the system perforated plate-back cavity are planar. The reflection coefficient is calculated at four positions above the aperture center, at $x = 70a,\ 80a,\ 90a$ and $95a$. The reflection coefficient at $x = 0$ (aperture outlet plane) is reconstructed, assuming that the acoustic field is a combination of two planar waves, one traveling downward (towards the plate) and the other upward (away from the plate). Results of the reconstructed reflection coefficient at $x = 0$ are shown to be identical (differences between the results coming from the four stations are less than 0.3%).

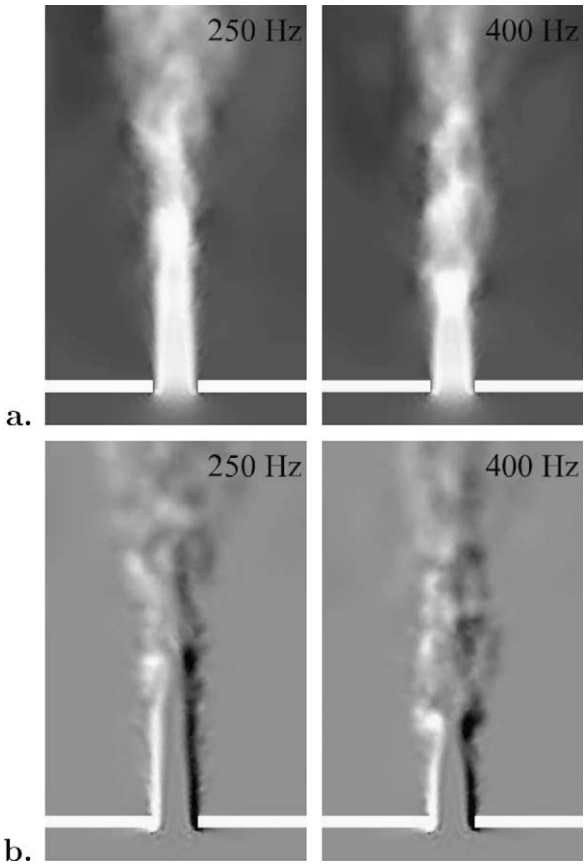

Fig. 2. Instantaneous solutions from the runs pulsed at 250 and 400 Hz: cutting plane $z = 0$. (a) Velocity field in the x direction from $-0.5\overline{U_j}$ (black) to $1.5\overline{U_j}$ (white). (b) Vorticity field in the z direction from $-3\overline{U_j}/a$ (black) to $3\overline{U_j}/a$ (white). Figure from Dassé et al. [10].

Fig. 3(a) presents the absorption coefficient A of the perforated plate as a function of the pulsing frequency f. The present LES results are reported, together with the experimental results of Bellucci et al. [2] and the numerical data of the JSM [19]. The theoretical Howe model is also plotted, together with its modified version accounting for the plate thickness (see Section 2.2).

All data provide the same form for the absorption coefficient. The presence of the perforated plate induces an acoustic absorption that depends on the frequency. The absorption is maximum around $f_m \approx 400$ Hz, resulting in an absorption peak in Fig. 3(a). For this frequency, almost all the incident acoustic wave is absorbed by the system. The LES results show the same behavior as the other data.

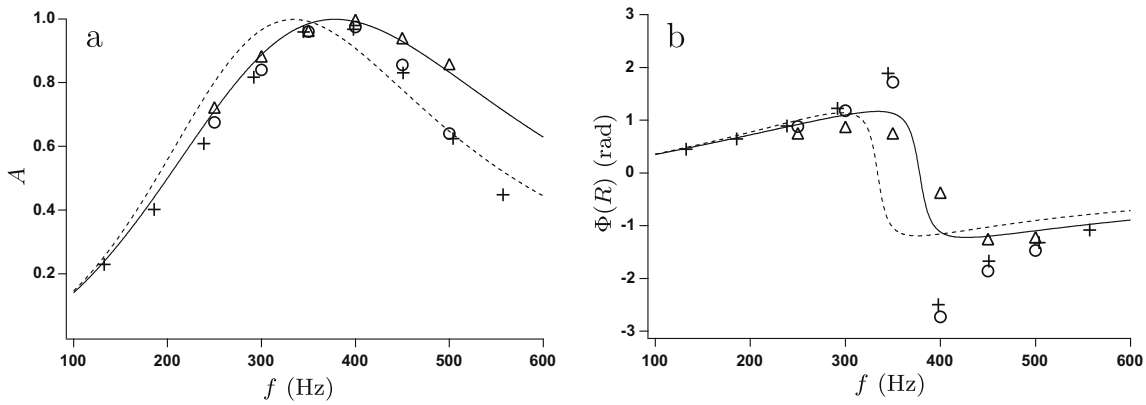

Fig. 3. Acoustic behavior of the system (perforated plate + cavity). (a) Absorption coefficient; (b) phase of the reflection coefficient. —: HM; – – –: MHM; +: results adapted from JSM; △: results adapted from Bellucci et al. [2]; ○: present LES results. Figure from Dassé et al. [10].

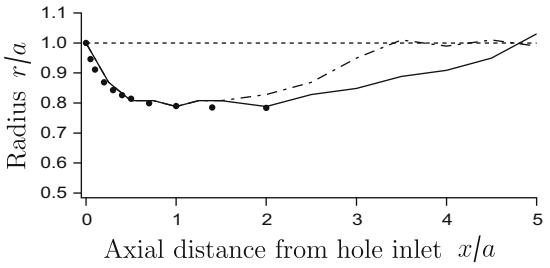

Fig. 4. Jet profile coordinates. Comparison of the numerical profile at $f = 400$ *Hz* (—) and $f = 500$ *Hz* (–·–·–) with the profile of Rouse and Abul-Fetouh [36] for a perforated plate porosity $\sigma = 0.0231$ (●) and the jet profile assumed by Howe [14] (- - -).

If the general form is the same for all the results and models, a more detailed comparison allows to highlight differences. It is possible to divide the results into two regions, depending on the frequency of excitation:

- For $f \leqslant f_m$, almost all data collapse. The HM and JSM give very similar absorption coefficient. The agreement with the experimental measurements of Bellucci et al. [2] is very good. At these low frequencies, the LES give values of absorption coefficient in excellent agreement with all these data. The MHM is the only one to give different results. In particular, the MHM under-predicts in this case the frequency of the absorption peak. At least for low frequencies, it is possible to conclude that the LES provides good values for the absorption coefficients.
- For $f > f_m$, two kinds of results are observed. The HM gives high values of absorption coefficient, in agreement with the results of Bellucci et al. [2]. On the contrary, the JSM and the MHM predict values of the absorption coefficient approximately 25 % lower. Concerning the models, it appears clearly that the plate thickness has a much higher effect on the results at high frequencies. Note that even if the plate thickness is moderate ($h/a = 0.5$), the correction in the MHM model is important after the absorption peak. The LES results show a very good agreement with the JSM, that accounts for the jet shape and the plate thickness. Surprisingly, even if the plate has a finite thickness, the experimental results of Bellucci et al. [2] are very close to the Howe model, that neglects this thickness.

Fig. 3(b) displays the phase of the reflection coefficient. The phase is close to zero at low frequencies, and increases almost linearly with the frequency. Near the absorption peak, variations are larger and the phase sign changes. Above f_m, the phase increases slowly. Again, all data give the same behavior, including the LES results. As for the absorption coefficient, all data give very similar results al low frequencies. However, near f_m, phase variations are much larger for the JSM and the LES results, which are in very good agreement for all the frequencies tested.

As a conclusion about acoustic reflection, the present LES give results very similar to the numerical model developed by Jing and Sun [19], that is the most sophisticated one (Section 2.2). Compared to the data of the reference experiment, the results also collapse for low frequencies, but discrepancies are observed at higher frequencies. This might be due to the difference of configuration between the experimental test rig and the numerical simulations which consider an infinite plate. However, the agreement with the JSM, both for the modulus and phase of the reflection coefficient, supports the quality of the present LES results.

The acoustic models presented in Section 2.2 are based on several hypotheses. Their accuracy can be verified in the numerical simulations. In particular, the HM, MHM and JSM assume a particular form for the jet. Fig. 4 displays the azimuthal-averaged jet profile coordinates in the LES for two frequencies of excitation, $f = 400$ and 500 Hz. The jet profile is determined from the position of the maximum of azimuthal vorticity. It is compared with the hypothesis of Howe (cylindrical vortex shedding) and the hypothesis of Jing and Sun (jet profile interpolated from the data provided by Rouse and Abul-Fetouh [36]). The abscissa is the axial distance from the hole inlet.

At the hole inlet, the jet separates from the rim and contracts. At the minimum, the jet radius corresponds approximately to $0.78a$. Further downstream, the jet progressively expands and then becomes turbulent (not shown). The agreement between the LES results at both frequencies of excitation and the Rouse and Abul-Fetouh profile is very good, especially at the beginning of the separation. This figure allows to explain the good agreement between the LES results and the JSM observed in Fig. 3. On the contrary the LES jet profile clearly departs from the form assumed by Howe [14]. The results of Figs. 3 and 4 clearly show the importance of the jet shape in the acoustic response of a perforated plate. As a consequence, even small differences in the hole geometry can lead to important differences on their acoustic behavior. Experiments on the acoustic behavior of perforated plates can for example be influenced by an imperfect drilling of the holes, in particular for small hole diameters.

3. Homogeneous model for multi-perforated plates in compressible LES codes

The former section has shown that LES is a suitable tool to generate data on the acoustic behavior of perforated plates. LES can thus be used for realistic configuration relevant to full-coverage film cooling in aeronautical gas turbines. However, if

such simulations are intrinsically interesting, for example to evaluate the influence of the aperture angle, the real interest is to manage to include the acoustic effect of perforated plates in full-scale LES of the flow in aeronautical gas turbines. The aim of this part is to propose a simple and practical model for LES, able to reproduce the global behavior of the analytical models presented in the former section, the Howe model and its modified version.

In full-scale 3D computations of the flow in a gas turbine combustion chamber, the simulation of the FCFC jets is out of reach of current computers. This is due to the number of perforations (approximately 10,000 perforations in some chambers) and to their size, the hole diameter being typically 0.5 mm. As a consequence, homogeneous models are needed to account for FCFC in full-scale computations to avoid the resolution of the flow near the wall. This statement is true for both RANS computations and LES. However, in LES, the temporal behavior of the models has to be treated with care. The purpose is now to discuss the aspects related to the acoustic behavior of homogeneous models. First, an existing homogeneous model based on a steady formulation is evaluated in terms of acoustic response. As it is unable to provide a realistic behavior in terms of acoustics, a modification is proposed and evaluated.

In all this section, plots on acoustic results (impedance, reflection coefficient, etc.) always include the data from the Howe model (HM) and the modified Howe model (MHM) presented in Section 2.2.

3.1. Existing coupled model

In a recent study [27], a uniform model has been proposed to treat both sides of the perforated plate. This model will be referred to as UM1 (Uniform Model 1) in the following. It allows to model both the suction and the injection of fluid depending on the side of the plate, replacing the perforated plate by two disjoint homogeneous boundary conditions. The boundary conditions representing the two sides of the wall are coupled so that the local mass flow rate that crosses the wall depends on the local distribution of pressure drop. The model reproduces the inviscid fluxes through the real perforated plate, that have been shown to be the first-order effect in FCFC configurations [28].

The performances of this model in terms of flow dynamics have been evaluated *a priori* [28] and *a posteriori* [27]. In the *a posteriori* validation, two channels are separated by a plate that is perforated over a certain portion. Using the model, both channels are disjoint and two homogeneous conditions replace the discrete suction/injection of fluid. To evaluate the mass flow rate through the perforated plate, a law for the discharge coefficient is prescribed. It relates the pressure drop through the plate to the bulk velocity in the hole through:

$$\Delta P = \frac{1}{2C_D^2}\rho U_j^2. \tag{9}$$

This model proves to provide satisfactory results in terms of flow dynamics in the two-channels configuration. It is well suited for RANS computations but the objective is also to use such a homogeneous model in LES of gas turbines combustion chambers potentially subjected to combustion instabilities. As stated before, perforated plates have an impact on acoustics and thus potentially on combustion instabilities. As a consequence, a useful model for LES of combustion instabilities has to provide a satisfactory acoustic behavior. To evaluate the acoustic behavior of the model, Eq. (9) is written in terms of bulk normal velocity through the homogeneous condition, U_W. α being the inclination angle of the apertures, $U_W = \sigma U_j \sin(\alpha)$. Eq. (9) becomes

$$\Delta P = \frac{1}{2C_D^2}\rho \frac{U_W^2}{\sigma^2 \sin^2(\alpha)}. \tag{10}$$

Assuming a small acoustic perturbation to the steady state, relation 10 is linearized. Perturbations are assumed to be harmonic (Eq. (1)).

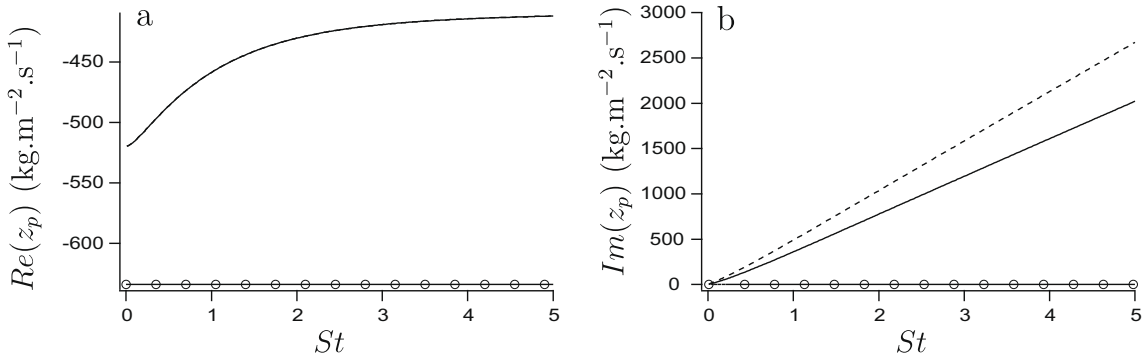

Fig. 5. Impedance jump of the homogeneous multi-perforated plate boundary condition. Comparison between UM1 (–○–), HM (—) and MHM (- - -). (a) Real part; (b) imaginary part.

It is straightforward to show that the impedance jump through the plate is (with $\overline{U_W}$ the time- and spatial-averaged velocity over the total wall surface)

$$z_p = -\frac{\rho\overline{U_W}}{\sigma^2 C_D^2 \sin^2(\alpha)}. \tag{11}$$

The main comment that can be made on this expression is that UM1 only provides a real impedance jump, with a zero imaginary part. Fig. 5 presents the real and the imaginary parts of the impedance of UM1: for the numerical applications in this section, the values of the Bellucci test case will be used in terms of geometry and operating point ($\rho = 1.2\ \mathrm{kg\ m^{-3}},\ \overline{U_W} = u^\infty \approx 0.115\ \mathrm{m\ s^{-1}},\ \sigma = 0.0231,\ C_D = 0.64,\ \alpha = 90^\circ$).

The real part of the impedance is constant in UM1, contrary to the Howe models (both the HM and the MHM have the same real part). The imaginary part is zero, which is very different from the HM and the MHM, for which the imaginary part of the impedance is approximately linear with the Strouhal number. From Fig. 5, errors in the acoustic behavior of the homogeneous model are expected to increase with the Strouhal number of the acoustic perturbation.

3.2. Broadband time-domain modeling of the acoustic response of multi-perforated plates

To improve the acoustic behavior of UM1, the relation that allows to calculate the mass flow rate as a function of the pressure drop is modified by adding a temporal dependance. This is inspired by the works by Cummings and Eversman [9] and Luong et al. [25]. Cummings and Eversman [9] use the Bernoulli's equation for unsteady flows to evaluate the acoustic transmission at the end of a converging nozzle, without mean flow. Luong et al. [25] also use it in the case of a perforated plate with bias flow in order to unify the approach for non-linear acoustic absorption described by Cummings and Eversman [9], Cummings [7,8] and Howe's linear model for the acoustic absorption in perforated plate with bias flow [14].

Eq. (12) describes the motion of fluid of volume $\Pi a^2 l'$ (l' being called the effective length and Πa^2 is the aperture area) and of mass $\rho\Pi a^2 l'$:

$$\Delta P = \rho l' \frac{\partial U_j}{\partial t} + \frac{\rho (U_j)^2}{2C_D^2}. \tag{12}$$

In terms of bulk velocity through the plate, Eq. (12) becomes:

$$\Delta P = \frac{\rho l'}{\sigma \sin(\alpha)} \frac{\partial U_W}{\partial t} + \frac{1}{2C_D^2} \rho \frac{U_W^2}{\sigma^2 \sin^2(\alpha)}. \tag{13}$$

By linearizing Eq. (13), one easily obtains the impedance jump associated with this model:

$$z_p = -\frac{\rho\overline{U_W}}{\sigma^2 C_D^2 \sin^2(\alpha)} + i\frac{\rho\omega l'}{\sigma \sin(\alpha)}. \tag{14}$$

The characteristic length l' has to be determined. This is extensively discussed by Luong et al. [25]. They chose $l' = \frac{\pi}{2}a + h$, which also corresponds to the value without bias flow. The value is different from the correlation obtained by Cummings [8], which is adapted to the cases without bias flow, where a jet is formed due to the pressure oscillations. Note that this expression for l' is consistent with the models presented in Section 2.2: in the HM, when $St \to \infty,\ K_R \to 2a$. In other words, $z_p \to i\frac{\rho\omega}{\sigma}\left(\frac{\pi}{2}a\right)$. In the MHM, which accounts for the plate thickness, $z_p \to i\frac{\rho\omega}{\sigma}\left(\frac{\pi}{2}a + h\right)$. By comparison with Eq. (14), it is shown that $l' = \frac{\pi}{2}a + h$ is consistent with models derived for linear acoustic absorption of perforated plates with bias flow.

The modified Howe model was derived for normal perforations. In the case of inclined perforations, Eldredge et al. [11] proposed to account for the aperture inclination in the modified Howe model using the aperture length instead of the plate thickness, viz. $l' = \frac{\pi}{2}a + \frac{h}{\sin(\alpha)}$. Note that they obtained even better comparisons between their numerical data and the model by adjusting l' as $l' = \frac{\pi}{2}a + 0.75\left(\frac{h}{\sin(\alpha)}\right)$ but this cannot be considered as a universal value.

To summarize, three expressions are available to couple the two sides of the homogeneous perforated wall. They are reported in Table 1. UM2 is a particular case of model UM3, with zero plate thickness. Note that models UM2 and UM3 have been tested in the stationary case used to validate UM1 in Mendez and Nicoud [27] and provide the same flow results as UM1.

Table 1
Summary of the homogeneous models.

Model name	Expression	Value of l'
UM1	$\Delta P = \frac{(\rho U_j)^2}{2\rho C_D^2}$	–
UM2	$\Delta P = \rho l' \frac{\partial U_j}{\partial t} + \frac{(\rho U_j)^2}{2\rho C_D^2}$	$\frac{\pi a}{2}$
UM3	$\Delta P = \rho l' \frac{\partial U_j}{\partial t} + \frac{(\rho U_j)^2}{2\rho C_D^2}$	$\frac{\pi a}{2} + \frac{h}{\sin(\alpha)}$

From Table 1, the differences between all models are limited to the temporal variations. This is why differences between models are only observed on the imaginary part of the impedance jump: Fig. 6 compares the impedance jump of the three models. The real part is not modified in UM2 and UM3 compared to UM1 but the imaginary part of models UM2 and UM3 is a good approximation of the HM and the MHM, respectively.

3.3. A posteriori testing of the uniform models: the Bellucci test case

These new boundary conditions with time dependence are implemented in the LES code AVBP. U_W^n and ΔP^n being respectively the wall-normal velocity through the homogeneous perforated wall and the pressure drop at iteration n, the velocity to impose U_W^{n+1} is calculated by developing the time derivative at the first order:

$$U_W^{n+1} = U_W^n + \frac{\sigma \sin(\alpha)\Delta t}{\rho l'}\left(\Delta P^n - \frac{1}{2C_D^2}\rho\frac{(U_W^n)^2}{\sigma^2\sin^2(\alpha)}\right). \tag{15}$$

The key point here is that we now obtain a model consistent with the family of complex impedances first derived by Howe [14]. The models with time dependence are easy to implement in an LES compressible code. They provide satisfactory results in terms of acoustic absorption, with necessitating any additional storage.

All models are compared in the Bellucci case (computational domain in Fig. 7). The perforated plate is replaced by the uniform models. The computational domain is then composed by two disjoint domains linked together with the coupled suction/injection boundary condition. As in the former section, the inlet is fully reflective and the outlet condition is pulsed. The computational domain is presented in Fig. 7. As the case is physically one-dimensional, the grid is hexahedral, regular and contains 40 hexahedral cells in the x direction (10 cells for the domain of length l and 30 for the domain of length L) and only 2 cells in the periodic directions. The Lax–Wendroff scheme (see Section 2.1.1) is used for the test cases.

Fig. 8 shows the results in terms of absorption coefficient and phase of the reflection coefficient for the proposed models of Table 1 (AVBP results and analytical curves). Fig. 8(a) and (b) compare UM1 and UM2 with the Howe model. Fig. 8(c) and (d) compare UM1 and UM3 with the modified Howe model.

The first comment concerns the exactness of the results provided by AVBP. For UM1, UM2 and UM3, the agreement between the simulation results (plain symbols) and the analytical formulas (lines with open symbols) derived to describe the acoustic behavior of the coupled multi-perforated plate boundary conditions is excellent.

UM1 gives results that can be completely different from the ones provided by the HM and the MHM. Trends are different and levels do not match at all, except for low Strouhal numbers (typically less than 0.5). Notably, the absorption coefficient using UM1 is higher than 0.8 above $St \approx 1.5$. It means that this model damps acoustic waves at amplitudes for which it should be slightly dissipative.

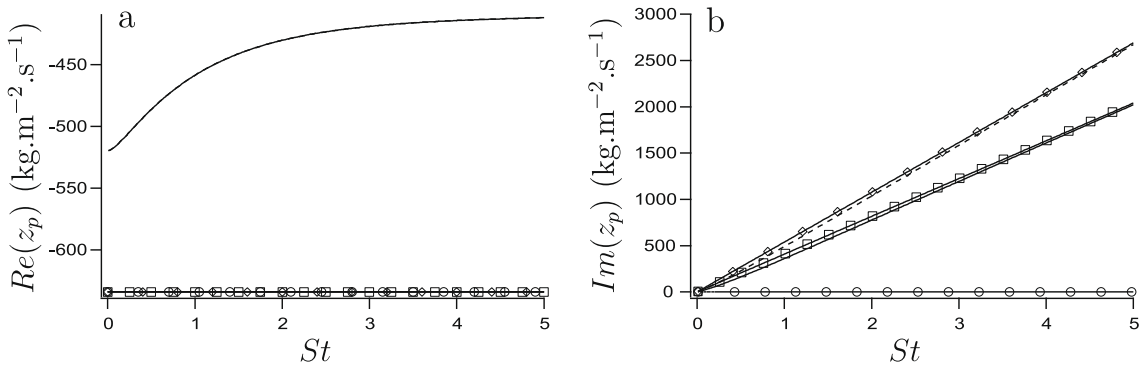

Fig. 6. Impedance jump of the homogeneous multi-perforated plate boundary conditions. Comparison between UM1 (–○–), UM2 (–□–), UM3 (–◇–), HM (—) and MHM (- - -). (a) Real part; (b) imaginary part.

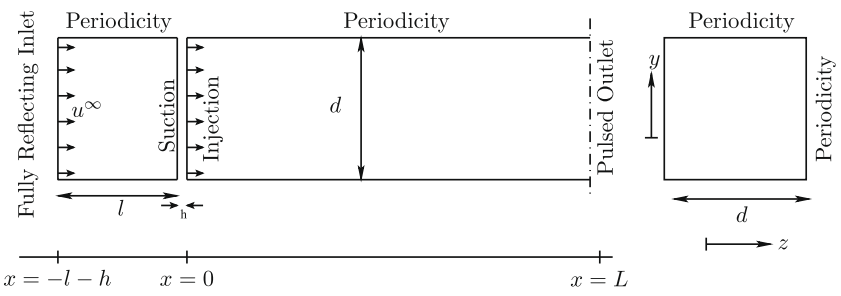

Fig. 7. Schematic of the computational domain in the LES testing the multi-perforated plate models.

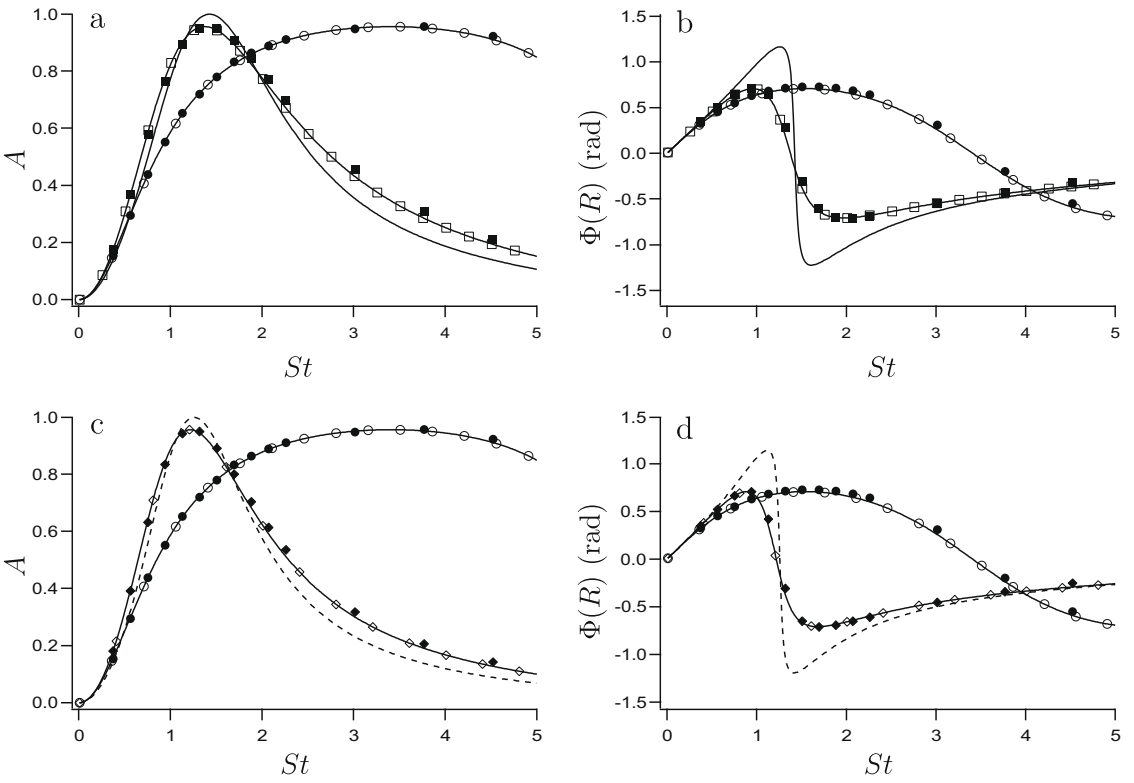

Fig. 8. Bellucci test case replacing the perforated plate by a homogeneous model. Comparisons of AVBP results using UM1 (●), UM2 (■) and UM3 (♦) and analytical results with UM1 (–○–), UM2 (–□–), UM3 (–◇–) and HM (—) and MHM (---). (a) Absorption coefficient for UM1, UM2 and HM; (b) phase of the reflection coefficient for UM1, UM2 and HM; (c) absorption coefficient for UM1, UM3 and MHM; (d) phase of the reflection coefficient for UM1, UM3 and MHM.

On the contrary, as expected from the impedance results, UM2 and UM3 reproduce a general behavior that is in rather good agreement with the Howe model and its modified version. UM2 has to be compared to the Howe model (Fig. 8(a) and (b)). Compared to the HM, UM2 slightly under-estimates the level of the peak absorption (Fig. 8(a)) but predicts correctly its Strouhal number (around $St = 1.5$). Except around the peak absorption, UM2 tends to over-estimate the absorption coefficient. Similar comments can be made for the comparison between UM3 and the modified Howe model (Fig. 8(c) and (d)).

Concerning the phase of the reflection coefficient (Fig. 8(b)), the agreement between UM2 and the Howe model is fair for low and high values of the Strouhal number. Around the peak absorption ($1.0 \leqslant St \leqslant 2.0$), variations for the Howe model are much stiffer and larger differences are observed. Again, similar conclusions can be drawn from the comparison between UM3 and the MHM (Fig. 8(c) and (d)).

The coupling condition for UM1 has provided satisfactory results in terms of steady dynamical behavior. However, its acoustic behavior is completely wrong. It cannot be used as it is in a predictive simulation of combustion instability in a gas turbine combustion chamber. This is not unexpected, as Eq. (9) neglects the inertia of the fluid submitted to unsteady perturbations. This is what correct the models UM2 and UM3. Indeed, the improvement of model UM1 in terms of prediction of acoustics is substantial. Trends are perfectly predicted with the new models. Results in terms of acoustic absorption are very good. Larger differences are observed on the phase of the reflection coefficient for Strouhal number values close to the peak absorption. This is discussed in next section.

3.4. Discussion

3.4.1. Comparison of UM2 and the Howe model

Compared to the Howe model, UM2 has an additional parameter, which is the discharge coefficient C_D. For a given average velocity, the real part of the impedance jump in model UM2 is independent of the Strouhal number but its level is determined by the discharge coefficient.

As stated by Howe [14], the Rayleigh conductivity in his model behaves like $2a(1 - i/St)$ when $St \to \infty$. By comparison with the limit behavior of UM2 (Eq. (14)), one finds that:

$$l' = \frac{\pi a}{2} \quad \text{and} \quad C_D^2 = \frac{2}{\pi}. \tag{16}$$

Eq. (16) shows that an analytical value for C_D can be derived in the limit of high Strouhal number values. This value is consistent with $C_D^2 \approx 0.64$, which corresponds to the experimental values obtained for the area contraction ratio through a diaphragm at high Reynolds number values (see for example Rouse and Abul-Fetouh [36]).

This value of discharge coefficient can be imposed in UM2. Outputs in terms of impedance jump and in the Bellucci configuration are displayed in Fig. 9.

The real part of z_p in UM2 corresponds to the asymptotic value of the Howe model (Fig. 9(a)). As seen before, the agreement is fair for the imaginary part (Fig. 9(b)). As a consequence, the results in the Bellucci test case show also a very good agreement. UM2 matches perfectly the absorption coefficient of the Howe model (Fig. 9(c)). Some discrepancies are observed on the phase of the reflection coefficient, near the peak absorption. Note that to obtain a closer agreement between UM2 and the Howe model, C_D should be chosen so that the real part of the impedance in UM2 matches the Howe model near the peak absorption (typically with $C_D^2 = 0.59$). $C_D^2 = 0.59$ is close to the value recommended by Cummings [8], who takes $C_D = 0.75$. This limit is consistent with that discussed by Luong et al. [25], who reconciled the Howe model with the non-linear model of Cummings.

This section has shown that the results obtained by Howe with his impedance model can be reproduced in the time-domain thanks to a model described by a simple and practical expression, referred to as UM2. A very fair agreement is obtained by using the limit behavior of the Howe model for high Strouhal numbers to evaluate the constants of model UM2. Note that in practice, the discharge coefficient is not a free parameter of UM2 and cannot be adjusted to match a target acoustic behavior: it is the hydrodynamic coefficient relating the average momentum flux through the hole to the pressure drop across the plate. This paragraph shows that it is possible to interpret the Howe model in terms of discharge coefficient: the Howe model implies a value for the discharge coefficient corresponding to what can be expected from an infinitely thin perforated plate, which corresponds to the hypothesis used by Howe to derive his model.

3.4.2. Effect of non-linearities

The models were tested in the linear regime in this paper. Luong et al. [25] evaluated the effect of non-linearities on the time-domain models. They found little effects of the amplitude of the pressure fluctuations on the acoustic response of a perforated plate. This is consistent with the experimental work by Tran [47].

From these two studies, it is possible to give a limitation for the time-domain models presented in this section: the effect of non-linearities is important only when the pressure fluctuations are higher than the mean pressure drop across the plate. In that case, pressure fluctuations are sufficient to obtain a reverse flow in the aperture. When strong reverse flow is

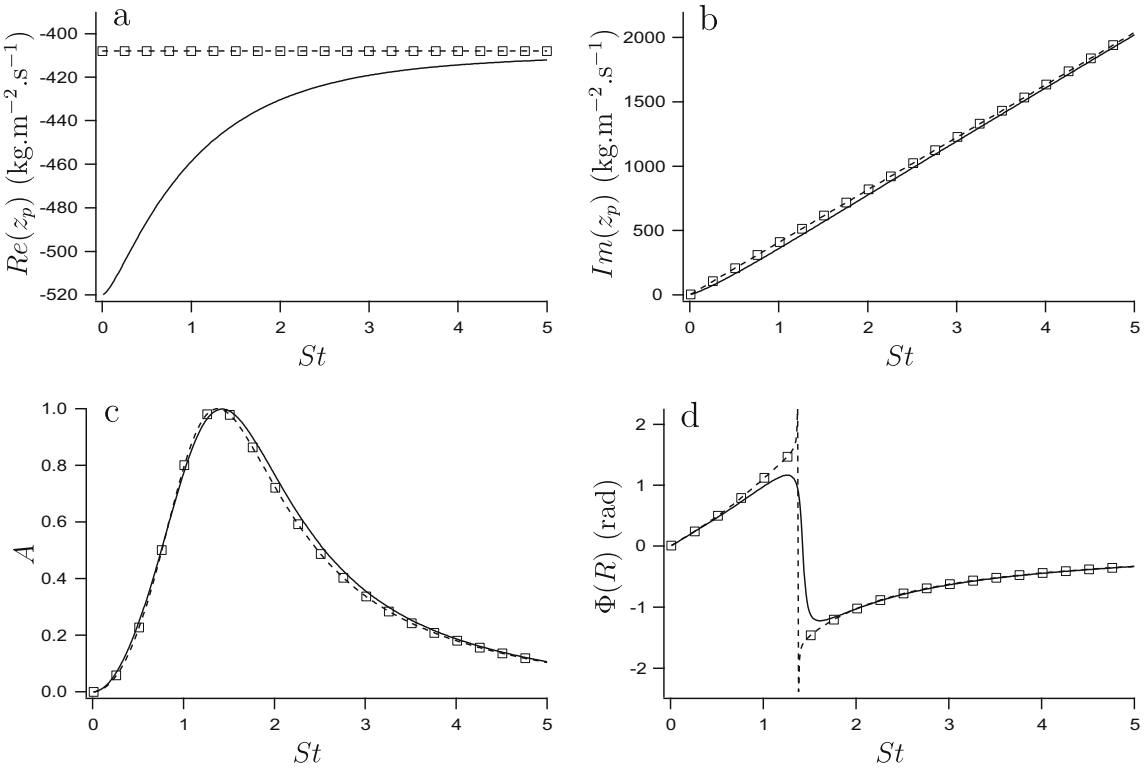

Fig. 9. Comparison between the HM (—) and UM2 with $C_D = \sqrt{2/\pi}$ (–□–). (a) Real part of the impedance jump; (b) imaginary part of the impedance jump; (c) Bellucci test case: absorption coefficient; (d) Bellucci test case: phase of the reflection coefficient.

promoted due to high acoustic fluctuations, the models presented in this paper are not valid any more. Notably the parameter l' used in models UM2 and UM3 should be changed to account for flow reversal in the aperture (see [8,25]). The reader is referred to the studies by Luong et al. [25] and Tran [47] for more extensive discussions about non-linear effects in the case of perforated plates with bias flow.

As a conclusion, models UM2 and UM3 can be used in a wide range of configurations. In aeronautical gas turbines combustion chambers for example, intense thermo-acoustic instabilities can generate pressure fluctuations of the same order as the pressure drop across the perforated plates, but they quite rarely promote strong reverse flow in the perforations.

4. Application of the model in a helicopter gas turbine combustor

4.1. Configuration of interest

In this section, the configuration of a real gas turbine chamber studied by Boudier et al. [4] is adapted to perform Large-Eddy Simulations in presence of perforated plates, using the coupled model UM3. The objective of this section is above all to show that the model is practical and can be used in a highly complex geometry. The comparison between models UM1 and UM3 is provided as an illustration of the results. Deeper analysis would be needed to evaluate the impact of changing the perforated plate model.

Fig. 10, coming from Boudier et al. [4], presents the configuration studied. It corresponds to an annular reverse-flow combustion chamber of a helicopter gas turbine. The combustor is fed with fuel by fifteen double-staged counter-rotating swirlers. The computational domain either focuses on a 24 degree section of the combustion chamber, designed by Turbomeca (SAFRAN group). It contains the liner, a fuel injection system and the casing. Walls are perforated in the intermediate zone and in the dome to be protected from the hot burnt gases. As the casing is also included in the calculations, perforated plates can be seen here as internal conditions. Therefore, the coupled models described by Mendez and Nicoud [27] are used, the local mass flow rate being imposed through the equations presented in the former section. Either models UM3 or UM1 will be used and compared.

LES are performed using AVBP, with the TTGC scheme [6]. The subgrid model is a classical Smagorinsky model [42]. The subgrid scale combustion terms have to be modeled in LES of turbulent reacting flows. The model employed here is the Dynamic Thickened Flame (DTF) model [5]. The unstructured mesh generated for the axi-periodic sector contains approximately 2,800,000 tetrahedral elements. Special attention is devoted to the primary zone and the swirler. As the aim is not to describe the combustion process in this chamber, the reader is referred to Boudier et al. [4] for more details about the combustion modeling, the numerical parameters, the mesh and the flow results.

The difference between the former calculations and the present calculations lie in the treatment of multi-perforated plates. In the former study, only the injection side of the plate (*i.e.* the side seen by the combustion chamber) was accounted for in the LES and suction sides were replaced by walls, the corresponding flow rate being subtracted from the compressor air inlet condition. In the present study, both sides of the multi-perforated walls are modeled and coupled. The mesh being unstructured, the pressure field is interpolated over the multi-perforated plate when applying the models. More specifically, at a given node located on a multi-perforated plate boundary condition, the pressure on the other side of the plate (used to calculate the pressure drop) is calculated by interpolating the values from three nodes. With 9000 nodes located on

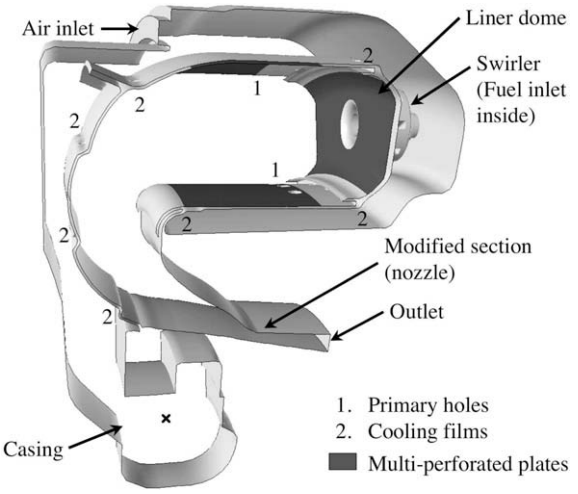

Fig. 10. Sector of the combustion chamber studied in this section. Locations of the multi-perforated plates are shown. **x** marks the location of the probe used to record pressure signals used in Fig. 11.

perforated walls boundary conditions, the computational cost increases by approximately 5% when using coupled boundary conditions. This is mainly due to the additional communications between processors needed when performing parallel computations.

4.2. Computational results

Two computations (S2 and S3) start from a converged solution obtained by Boudier et al. [4]. The calculation from Boudier et al. [4] is referred to as simulation S1 in the following. Coupled multi-perforated plates boundary conditions are imposed, either using UM1 (simulation S2) or UM3 (simulation S3). In the following, results from S1 will be used and compared qualitatively to the results from S2 and S3. However, it has to be reminded that in S1, only the injection side of the perforated walls was accounted for, with the mass flow rate imposed, while in S2 and S3, both sides are included, with models UM1 and UM3 used to calculate the mass flow rate, respectively.

All simulations are subject to a thermo-acoustic instability already described by Boudier et al. [4], of period T_i in S1. As will be shown, the frequency of the instability slightly changes in simulations S2 and S3. At Turbomeca's request, no dimensional values are provided. To make the quantities non-dimensional, characteristics of the jets issuing from the effusion cooling plates are used. Using the hole diameter and an average bulk velocity through the holes in the whole chamber, the Strouhal number of the thermo-acoustic instability is $St_i \approx 0.0028$, which is small. Simulations S2 and S3 are run during $80T_i$. Post-processing is made on numerical data gathered over $40T_i$, which is comparable to data from simulation S1.

In terms of time-averaged behavior, the mass flow rate passing through the perforated plates is identical in simulations S2 and S3. Changing the coupling mode of the multi-perforated plate does not modify the time-averaged behavior of the flow. On the contrary, small effects can be observed on the unsteady flow behavior. Before showing the results, it proves useful to remind that the Strouhal number of the instability is small. More precisely, the difference in absorption coefficient and phase at this Strouhal number for the perforated plates considered in the calculation are less than one percent. As a consequence, results are not expected to be very different using either models UM1 or UM3. Moreover, values of absorption coefficient are small for such low Strouhal number.

Fig. 11 shows the power spectral density (PSD), in arbitrary units, of the temporal pressure signal recorded in the casing, at the probe shown in Fig. 10. In Fig. 11(a), results from Boudier et al. [4] are included for simulation S1. In order to compare S2 and S3, Fig. 11(b) presents a zoom in the frequency range of instability. Note first that the results obtained for simulations S2 and S3 are rather noisy and show some low-frequency variations. Additional calculation time would be needed to obtain cleaner results. However, they are sufficient for the objectives we want to reach.

First, both simulations using coupled two-side multi-perforated walls are clearly distinct from simulation S1 (Fig. 11(a)). While the three simulations exhibit high values of PSD for $0.0025 < St < 0.0035$, S1 has a much higher peak. The instability is much stronger in simulation S1. Furthermore, the frequency of the instability is slightly higher in simulations S2 and S3. It is difficult to isolate the exact phenomenon that modifies the intensity of the instability between S1 and S2 or S3, as the latter simulations account for the suction sides of the walls *and* the coupling between both sides of the wall. However, it can be said that neglecting the perforated walls when predicting thermo-acoustic instabilities in gas turbines combustion chamber can have an effect on the results.

Both simulations S2 and S3 show the same structure for the spectrum measured in the casing (see Fig. 11(b)). Notably, they both have a broad peak at $0.0028 < St < 0.0035$ (actually composed by two close peaks). This means that the perforated plates used to cool the walls do not have a sufficient acoustic absorption effect to completely damp the instability. However, the intensity of the instability is much lower when accounting for the presence of perforated plates (simulations S2 and S3).

Another comment that can be made about Fig. 11(b) is that the use of UM1 or UM3 does slightly change the results. Even if the difference between the acoustic characteristics of the models could be considered as negligible for the range of fre-

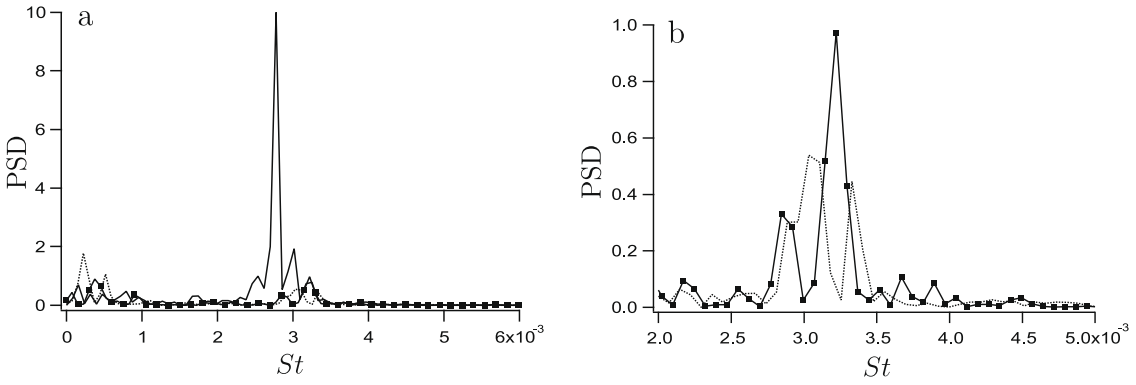

Fig. 11. Non-dimensional power spectral density (PSD), in arbitrary units, of the pressure fluctuations signals recorded in the casing at the probe shown in Fig. 10. (a) Comparison for runs S1 (—), S2 (using model UM1, (–■–) and S3 (using model UM3, ···); (b) zoom to compare runs S2 and S3.

quencies considered, the impact on the flow results is not negligible. Notably, the frequency of the instability peaks is slightly shifted depending on the perforated plate model used. Of course, these results should be considered with a lot of care, as the duration of the pressure record is not sufficient to draw definitive conclusions. However, as the *only* difference between the two calculations is the perforated plate model, it is clearly seen that the wall model should account for inertia even at low Strouhal numbers.

5. Conclusion

In the context of flow predictions in gas turbine combustors by Computational Fluid Dynamics, accounting for full-coverage film cooling seems unavoidable. But in the particular case of Large-Eddy Simulations (LES), the unsteady behavior of models for perforated plates has to be treated with care, to correctly represent their impact on acoustic waves. This is particularly true when the chamber is subjected to thermo-acoustic instabilities. The present study was focused on LES of the flow around perforated plate, with and without resolution of the holes, in presence of acoustic perturbations. Two aspects were treated: the ability of resolved LES to provide reliable results of the acoustic behavior of a perforated plate submitted to an acoustic perturbation and the possibility to model this behavior through homogeneous boundary conditions.

LES proves to be able to reproduce the acoustic behavior of a perforated plate. The present results show the strong relation between the dynamic field and the acoustic response of the system. The acoustic results are in excellent agreement with the numerical model of Jing and Sun, that accounts both for the finite thickness of the plate and the particular shape of the jet after its separation from the aperture inlet rim. From the LES results, it is possible to get insight into the mechanisms that lead to acoustic absorption and to verify the assumptions made by the theoretical models. For example, our simulations show that the hypothesis of the Jing and Sun model concerning the jet shape seems to be relevant, at least at moderate Reynolds numbers. Detailed flow field information is missing about acoustic–vortex interactions in the case of perforated plates and numerical simulations offer a way to a deeper understanding of the small-scale flow physics.

Concerning the homogeneous modeling of multi-perforated plates, focus was made on how to determine the velocity in the direction normal to the plate, knowing the local flow conditions on each side of the plate. In a previous study, Luong et al. [25] have established the ability of a simple model, derived from the unsteady form of the Bernoulli's equation, to reproduce the complex effect of acoustic damping by perforated plates. In the present study, this model was shown to be practical for LES in presence of perforated plates. Results were presented in the configuration calculated in the first part of the paper, with an excellent agreement between numerical and analytical results. The difference between using a steady or an unsteady formulation of the Bernoulli equation to determine the normal velocity through the plate is treated with particular attention. Notably, it is shown that for low Strouhal number values, accounting for the fluid inertia has only a small effect, while this is crucial for high Strouhal number values. However, the limit between 'low' and 'high' values totally depends on the geometrical and average dynamical parameters of the flow.

As a proof of the interest and the robustness of the model, an example of application is given by calculating with compressible LES the flow in an actual gas turbine combustion chamber, in which a large portion of the walls are perforated. No particular stability problems have been seen when coupling both sides of the perforated plates with the equation presented in this paper. The preliminary results presented in this paper show expected behavior (acoustic damping of the instability compared to the case where perforated plates are not accounted for, comparable levels of acoustic activity using the steady or the unsteady model due to the low value of Strouhal number). It has been demonstrated that one should account for the presence of multi-perforated plates when calculating the flow in a combustion chamber subjected to a thermo-acoustic instability. Simulations have also shown that even for low values of the Strouhal number, the temporal term should not be neglected, as it may have an effect an the acoustic field.

Acknowledgments

The authors are grateful to the CINES (Centre Informatique National pour l'Enseignement Supérieur) and the BSC (Barcelona Supercomputing Center) for the access to supercomputer facilities. The authors would also like to thank Jean Dassé and Gregory Millot for their contributions and Franck Nicoud for his helpful comments and suggestions throughout this study. Finally, Guillaume Boudier, Laurent Gicquel and Turbomeca are gratefully acknowledged for providing the initial simulation of the helicopter gas turbine chamber.

References

[1] D.W. Bechert, Sound absorption caused by vorticity shedding, demonstrated with a jet flow, in: American Institute of Aeronautics and Astronautics, Aeroacoustics Conference, Fifth, Seattle, Wash., March 12–14, 1979, p. 11.
[2] V. Bellucci, P. Flohr, C.O. Paschereit, Numerical and experimental study of acoustic damping generated by perforated screens, AIAA Journal 42 (8) (2004) 1543–1549.
[3] G. Boudier, L.Y.M. Gicquel, T. Poinsot, Effect of mesh resolution on large eddy simulation of reacting flows in complex geometry combustors, Combustion and Flame 155 (1–2) (2008) 196–214.
[4] G. Boudier, N. Lamarque, G. Staffelbach, L.Y.M. Gicquel, T. Poinsot, Thermo-acoustic stability of a helicopter gas turbine combustor using Large Eddy Simulations, International Journal of Aeroacoustics 8 (1) (2009) 69–94.
[5] O. Colin, F. Ducros, D. Veynante, T. Poinsot, A thickened flame model for large eddy simulations of turbulent premixed combustion, Physics of Fluids 12 (7) (2000) 1843–1863.

[6] O. Colin, M. Rudgyard, Development of high-order Taylor–Galerkin schemes for unsteady calculations, Journal of Computational Physics 162 (2) (2000) 338–371.
[7] A. Cummings, Acoustics nonlinearities and power losses at orifices, AIAA Journal 22 (6) (1984) 786–792.
[8] A. Cummings, Transient and multiple frequency sound transmission through perforated plates at high amplitude, The Journal of the Acoustical Society of America 79 (1986) 942–951.
[9] A. Cummings, W. Eversman, High amplitude acoustic transmission through duct terminations: theory, Journal of Sound and Vibration 91 (4) (1983) 503–518.
[10] J. Dassé, S. Mendez, F. Nicoud, Large-eddy simulation of the acoustics response of a perforated plate, in: Proceedings of the 14th AIAA/CEAS Aeroacoustics Conference, AIAA-Paper 2008-3007, Vancouver, Canada, May 5–7, 2008.
[11] J.D. Eldredge, D.J. Bodony, M. Shoeybi, Numerical investigation of the acoustic behavior of a multi-perforated liner, in: Proceedings of the 13th AIAA/CEAS Aeroacoustics Conference, AIAA Paper 2007-3683, Rome, May 21–23, 2007.
[12] J.D. Eldredge, A.P. Dowling, The absorption of axial acoustic waves by a perforated liner with bias flow, Journal of Fluid Mechanics 485 (2003) 307–335.
[13] K. Fung, H. Ju, B. Tallapragada, Impedance and its time-domain extensions, AIAA Journal 38 (1) (2000) 30–38.
[14] M.S. Howe, On the theory of unsteady high Reynolds number flow through a circular aperture, Proceedings of the Royal Society of London Series A 366 (1979) 205–223.
[15] M.S. Howe, Acoustics of Fluid–Structure Interaction, Cambridge University Press, 1998.
[16] M.S. Howe, M.I. Scott, S.R. Sipcic, The influence of tangential mean flow on the Rayleigh conductivity of an aperture, Proceedings of the Royal Society of London Series A 452 (1997) 2303–2317.
[17] I. Hughes, A. Dowling, The absorption of sound by perforated linings, Journal of Fluid Mechanics 218 (1990) 299–335.
[18] X. Jing, X. Sun, Experimental investigations of perforated liners with bias flow, The Journal of the Acoustical Society of America 106 (5) (1999) 2436–2441.
[19] X. Jing, X. Sun, Effect of plate thickness on impedance of perforated plates with bias flow, AIAA Journal 38 (9) (2000) 1573–1578.
[20] X. Jing, X. Sun, J. Wu, K. Meng, Effect of grazing flow on the acoustic impedance of an orifice, AIAA Journal 39 (8) (2001) 1478–1484.
[21] S. Lee, J. Ih, K. Peat, A model of acoustic impedance of perforated plates with bias flow considering the interaction effect, Journal of Sound and Vibration 303 (3–5) (2007) 741–752.
[22] A.H. Lefebvre, Gas Turbines Combustion, Taylor and Francis, 1999.
[23] T. Lieuwen, V. Yang, Combustion instabilities in gas turbine engines, Operational Experience, Fundamental Mechanisms and Modeling, vol. 210, Progress in Astronautics and Aeronautics AIAA, 2005.
[24] M. Lohrmann, H. Buechner, Prediction of stability limits for LP and LPP gas turbine combustors, Combustion Science and Technology 177 (12) (2005) 2243–2273.
[25] T. Luong, M.S. Howe, R.S. McGowan, On the rayleigh conductivity of a bias-flow aperture, Journal of Fluids and Structures 21 (2005) 769–778.
[26] C. Martin, L. Benoit, Y. Sommerer, F. Nicoud, T. Poinsot, LES and acoustic analysis of combustion instability in a staged turbulent swirled combustor, AIAA Journal 44 (4) (2006) 741–750.
[27] S. Mendez, F. Nicoud, Adiabatic homogeneous model for flow around a multiperforated plate, AIAA Journal 46 (10) (2008) 2623–2633.
[28] S. Mendez, F. Nicoud, Large-eddy simulation of a bi-periodic turbulent flow with effusion, Journal of Fluid Mechanics 598 (2008) 27–65.
[29] V. Moureau, G. Lartigue, Y. Sommerer, C. Angelberger, O. Colin, T. Poinsot, Numerical methods for unsteady compressible multi-component reacting flows on fixed and moving grids, Journal of Computational Physics 202 (2) (2005) 710–736.
[30] F. Nicoud, L. Benoit, C. Sensiau, Acoustic modes in combustors with complex impedances and multidimensional active flames, AIAA Journal 45 (2) (2007) 426–441.
[31] F. Nicoud, F. Ducros, Subgrid-scale stress modelling based on the square of the velocity gradient tensor, Flow, Turbulence and Combustion 62 (3) (1999) 183–200.
[32] C. Pierce, P. Moin, Progress-variable approach for large eddy simulation of non-premixed turbulent combustion, Journal of Fluid Mechanics 504 (2004) 73–97.
[33] T. Poinsot, S.K. Lele, Boundary conditions for direct simulations of compressible viscous flows, Journal of Computational Physics 101 (1) (1992) 104–129.
[34] T. Poinsot, D. Veynante, Theoretical and Numerical Combustion, second ed., R.T. Edwards, 2005.
[35] C. Prière, L.Y.M. Gicquel, A. Kaufmann, W. Krebs, T. Poinsot, LES predictions of mixing enhancement for jets in cross-flows, Journal of Turbulence 5 (2004) 005.
[36] H. Rouse, A. Abul-Fetouh, Characteristics of irrotational flow through axially symmetric orifices, Journal of Applied Mechanics 17 (1950) 421–426.
[37] A. Roux, L.Y.M. Gicquel, Y. Sommerer, T. Poinsot, Large eddy simulation of mean and oscillating flow in a side-dump ramjet combustor, Combustion and Flame 152 (1–2) (2008) 154–176.
[38] P. Schmitt, T. Poinsot, B. Schuermans, K. Geigle, Large-eddy simulation and experimental study of heat transfer, nitric oxide emissions and combustion instability in a swirled turbulent high-pressure burner, Journal of Fluid Mechanics 570 (2007) 17–46.
[39] T. Schönfeld, M. Rudgyard, Steady and unsteady flows simulations using the hybrid flow solver AVBP, AIAA Journal 37 (11) (1999) 1378–1385.
[40] L. Selle, G. Lartigue, T. Poinsot, R. Koch, K.-U. Schildmacher, W. Krebs, B. Prade, P. Kaufmann, D. Veynante, Compressible large-eddy simulation of turbulent combustion in complex geometry on unstructured meshes, Combustion and Flame 137 (4) (2004) 489–505.
[41] C. Sensiau, F. Nicoud, T. Poinsot, A tool to study azimuthal standing and spinning modes in annular combustors, International Journal of Aeroacoustics 8 (1) (2009) 57–68.
[42] J. Smagorinsky, General circulation experiments with the primitive equations: I. The basic experiment, Monthly Weather Review 91 (1963) 99–164.
[43] Y. Sommerer, D. Galley, T. Poinsot, S. Ducruix, F. Lacas, D. Veynante, Large eddy simulation and experimental study of flashback and blow-off in a lean partially premixed swirled burner, Journal of Turbulence 5 (2004).
[44] X. Sun, X. Jing, H. Zhang, Y. Shi, Effect of grazing-bias flow interaction on acoustic impedance of perforated plates, Journal of Sound and Vibration 254 (3) (2002) 557–573.
[45] C.K.W. Tam, L. Auriault, Time-domain impedance boundary conditions for computational aeroacoustics, AIAA Journal 34 (5) (1996) 917–923.
[46] C.K.W. Tam, K.A. Kurbatskii, K.K. Ahuja, R.J. Gaeta, A numerical and experimental investigation of the dissipation mechanisms of resonant acoustic liners, Journal of Sound and Vibration 245 (3) (2001) 545–557.
[47] N. Tran, Influence de la condition limite acoustique amont sur les instabilités de combustion de grande amplitude: conception d'un système robuste de contrôle d'impédance, Ph.D. Thesis, Ecole Centrale Paris, 2009.
[48] N. Tran, S. Ducruix, T. Schuller, Analysis and control of combustion instabilities by adaptive reflection coefficients, in: Proceedings of the 13th AIAA/CEAS Aeroacoustics Conference, AIAA Paper 2007-3716, Rome, May 21–23, 2007.